Orthorhombic-tetragonal phase transition induced by Ta isovalent doping and its effect on fatigue characteristics of KNL-NST$_x$ ceramics

O. Namsar[a], C. Uthaisar[a], J. Glaum[b], S. Pojprapai[a,*]

[a] *School of Ceramic Engineering, Institute of Engineering, Suranaree University of Technology, 111 University Avenue, Muang, Nakhon Ratchasima 30000, Thailand*

[b] *Department of Materials Science and Engineering, Norwegian University of Science and Technology, 7491, Norway*

* Corresponding author. Tel.: +66 44224542

E-mail address: soodkhet@g.sut.ac.th (S. Pojprapai).

ABSTRACT

The effect of Ta addition on the bipolar fatigue characteristics of lead-free KNL-NST$_x$ ceramics (x = 0, 0.04, 0.07 and 0.11 mol%) is studied throughout 1 x 10^6 cycles. Bipolar cycling leads to a strong degradation of polarization in the unmodified KNL-NS ceramic which is due to the observed microstructural cracks as a result of a large domain wall pinning effect. Surprisingly, the fatigue endurance is improved after xTa dopant is incorporated into KNL-NS ceramics. This can be explained by reducing domain wall pinning due to oxygen vacancies. A low density of pinned domains gives less local internal stress, reducing the probability of crack formation and hence higher fatigue resistance. In order to understand the fatigue mechanism, a model of domain wall movement (domain switching)-oxygen vacancy accumulation is proposed. This

model is expected to guide future fatigue studies which concern novel lead-free KNN-based materials.

Keywords: Fatigue; Ferroelectric properties; Perovskites; Surfaces; X-ray methods.

1. Introduction

Ferroelectric materials are of great interest because they exhibit piezoelectric, dielectric, pyroelectric and ferroelectric properties [1]. These materials have been extensively applied in many electronic applications such as sensors, capacitors, actuators, ferroelectric memories etc. In actuator and memory applications, ferroelectric materials are usually operated under cyclic electrical loading [2,3]. Under these conditions, the long-term stability in terms of the fatigue lifetime of these ferroelectric devices has to be considered.

A popular ferroelectric material commonly applied in electronic applications is perovskite-type lead zirconate titanate (PZT). PZT has excellent piezoelectric, dielectric and ferroelectric characteristics [1]. However, it has poor fatigue resistance and is a toxic lead-based compound [4,5]. Many investigators have been developing alternative lead-free materials to replace PZT. Potassium sodium niobate (KNN) is one of most important lead-free ferroelectric materials, which retains the perovskite structure. Compared to PZT, however, KNN has relatively low piezoelectric performance and is difficult to fabricate, which makes it unattractive for practical applications [6]. Recently developed modified KNN-based materials doped with Li and Sb (abbreviated as KNL-NS) show high piezoelectric coefficients due to the shift of the polymorphic phase transition (PPT) [7,8]. However, the disadvantage of KNL-NS is poor fatigue resistance. The fatigue behavior of KNL-NS was reported by Zhang *et al.* [9]. They showed that

the polarization decreased by about 50% of its initial value after 200 cycles. Recently, some research works reported that the addition of a small amount of Ta dopant in KNL-NS (denoted as KNL-NST) can improve the piezoelectric coefficient of undoped KNL-NS ceramic [8,10]. Although they have reported on the piezoelectric properties of KNL-NST, there is a lack of understanding of the ferroelectric fatigue behavior. Therefore, the purpose of this work is to study the effect of Ta addition on the fatigue endurance of KNL-NS ceramic. This research will bring more understanding of the fatigue mechanism of this new lead-free ceramic.

2. Experimental procedure

Lead free $(K_{0.44}Na_{0.41}Li_{0.04})(Nb_{0.85-x}Sb_{0.04}Ta_x)O_3$ ceramics or KNL-NST$_x$ with x = 0, 0.04, 0.07 and 0.11 mol% were prepared by a conventional solid-state mixed-oxide reaction and sintered at 1130°C for 4 h dwell time. More detailed descriptions of ceramic processing are presented thoroughly in the previous publication [11].

Before the electrical fatigue test, the samples were prepared in the following way: Firstly, both surfaces of the pellet-shaped samples were ground to approximately 1 mm thickness and polished with fine SiC paper of 2000 grid to make the surfaces flat, smooth and parallel for measurements. In order to observe the influence of electrical fatigue on the microstructure, a small curve of the sample was then cut and polished to mirror finish with alumina paste of 0.02 μm. After that, silver paste was painted on both surface sides of the samples and dried at 200°C for 20 min in order to ensure the contact between the electrodes and the sample surfaces. The samples were poled under a DC field of 25 kV/cm for 20 min in a silicone oil bath at 200°C. The KNL-NST samples were then fatigued up to 1×10^6 switching cycles under the bipolar sinusoidal electrical load at 25 kV/cm of amplitude and 50 Hz of frequency. A conventional

Sawyer-Tower circuit was applied for fatigue measurement in this work [12]. The polarization-electric field (*P*-*E*) loops were recorded at different number of switching cycles. The remanent polarization ($2P_r$) was extracted from the *P*-*E* loops. Phase evolution of the ceramics before poling, after poling and after fatigue was also studied by using X-ray diffraction technique (XRD) (BLUKER AXS-D5005). The change of microstructure before and after fatigue test of the ceramic samples was examined by a scanning electron microscope (SEM) (JEOL-5800).

3. Results and discussion

Since the crystal structure plays an important role in the fatigue behavior of ferroelectric materials [13], a structural analysis of KNL-NST$_x$ ceramics is performed. Diffraction peaks at 44 – 48° of all compositions are observed as shown in Fig. 1(a). It is well accepted that the analysis of the relative intensity of the two peaks around $2\theta = 45°$ in XRD patterns is an effective method to distinguish the phase structure of KNN-based piezoelectric materials that usually possess orthorhombic and/or tetragonal symmetry at room temperature [14]. The tetragonal phase can be identified by splitting of the (002)/(200) peak (JCPDS file no. 71-0945 [15]) while the orthorhombic phase is characterized by splitting in the (202)/(002) peak (JCPDS file no. 71-2171 [16]). If the ceramic has a tetragonal phase, the intensity of the (002) should be greater than that of the (200). If the ceramic contains an orthorhombic phase the intensity of the (202) peak is greater than that of the (020) [17-22]. In addition, a coexistence of orthorhombic and tetragonal phases is expected to exist in the sample when the intensity of (002) or (202) peak is almost equal to the (200) or (020) one [10,14,20,23,24]. Therefore, the two XRD peaks around $2\theta = 45°$ are then fitted as shown in Fig. 1(a) and their relative intensities are also compared as listed in Table 1. XRD patterns of an unmodified KNL-NS sample ($x = 0$) correlated with an

orthorhombic structure. This is evident by a split in the (202)/(020) peak where the intensity of (202) is higher than that (020) peak with the intensity ratio of 1.4. When x = 0.04Ta is incorporated into KNL-NS, there is a coexistence of ferroelectric orthorhombic and tetragonal phases, which can be observed by an equal intensity of the peak at lower angle and the peak at higher angle with an intensity ratio of 1.0. The structure changes to tetragonal symmetry with further increase of x to 0.11, which is confirmed by (002)/(200) peak splitting where the intensity of (200) is weaker than that of (002) peak. In-depth consideration of XRD spectra, the slight shift in peak positions is also observed for all samples with xTa addition as compared to an undoped sample. This could be caused by the change of crystal structure parameters in these ceramics. Therefore, the variation of crystal structure parameters including lattice parameters (*a, b, c*), unit cell volume (*V*), *c/a* and *b/a* ratios of all composition is analyzed as illustrated in Fig. 1(b). Values of crystal structure parameters are also listed in Table 1. However, the crystal structure parameters of x = 0.04 sample are not calculated due to orthorhombic-tetragonal coexistence. As shown in Fig. 1(b) and Table 1, it can be seen that the structure of the ceramics transforms from orthorhombic to tetragonal symmetry with increasing Ta content. This can be observed by the reduction of unit cell volume and *b/a* ratio as well as an increase of *c/a* ratios. Based on the X-ray results, the phase transitional behavior and the shift of XRD peaks are observed. It is expected that the Ta^{5+} dopants dissolve into the perovskite KNL-NS crystal lattice [25]. The ionic radius of Ta^{5+} ions (0.64 Å) is similar to that of Nb^{5+} ions, but slightly bigger than Sb^{5+} ions (0.60 Å). Hence, Ta^{5+} ions would enter into Nb^{5+} or Sb^{5+} sites, leading to a phase transformation and a distortion of structure. This result is in good agreement with previous works [24], which reported that the B-site of KNNL was substituted by the Ta dopant. It is proposed that the phase

transformation is due to Ta incorporation, which affects the fatigue performance of KNL-NST$_x$ ceramics.

Fig. 2 depicts the polarization hysteresis loop of unmodified KNL-NS and Ta doped KNL-NS samples at three different cycling steps i.e. 1, 5 x 10^4 and 1 x 10^6 cycles. It is observed that bipolar electric fatigue causes a dramatic change in the hysteresis loop of all ceramics both in terms of shape and size. It is well known that the change of remanent polarization is a parameter which indicates the degradation of ferroelectric behavior due to electrical fatigue [26]. To compare the fatigue degradation rate of KNL-NST$_x$ samples, therefore, the $2P_r$ values are normalized by equation 1.

$$\text{Normalized } 2P_r = \frac{2P_r(N)}{2P_r(0)} \quad (1)$$

where, $2P_r(N)$ is the remanent polarization after N cycles and $2P_r(0)$ is the initial remanent polarization.

The average normalized $2P_r$ is then plotted as a function of electric cycling numbers, as provided in Fig. 3. It can be seen that all ceramic samples show a similar trend. The normalized $2P_r$ start to reduce at 5 x 10^3 then rapidly drop off at 1 x 10^6. However, there is a variation in the percentage decrease in normalized $2P_r$ drop off as shown in the inset graph. It can be seen that the composition with $x = 0$ (KNL-NST) shows a strong reduction of the normalized $2P_r$ (~88% of its unfatigued value), suggesting that this sample has low fatigue resistance. This significant fatigue of the unmodified KNL-NST sample could be due to the effect of the defect accumulations. This sample is considered to be an isovalent substitution due to the substituting of ions of the same charge (same oxidation state), as such there is no formation of point defect vacancies as a result of charge compensation. Based on an ionic radius comparison [25], Li^+ ions

(I_R = 0.76 Å) would replace the A-site ions (i.e. K^+ (I_R = 1.38 Å) and Na^+ (I_R = 1.02 Å)). On the other hand, Sb^{5+} (I_R = 0.70 Å) would enter into Nb^{5+} (I_R = 0.64 Å) which is the B-site ion. These substitutions can be written using the Kröger–Vink notation by:

$$Li_2O \xrightarrow{KNN} 2Li^{x}_{K\ or\ Na} + O^{x}_{O} \quad (2)$$

$$Sb_2O_5 \xrightarrow{KNN} 2Sb^{x}_{Nb} + 5O^{x}_{O} \quad (3)$$

Unfortunately, the volatile nature of potassium (K) and sodium (Na) leads to the creation of A-site cation and oxygen vacancies in the KNN-based materials during high temperature processing [27]. The reactions may be explained in term of Kröger–Vink notation with the following equations:

$$2K^{x}_{K} + O^{x}_{O} \rightleftharpoons 2V'_{K} + V^{\bullet\bullet}_{O} + K_2O\ (g) \quad (4)$$

$$2Na^{x}_{Na} + O^{x}_{O} \rightleftharpoons 2V'_{Na} + V^{\bullet\bullet}_{O} + Na_2O\ (g) \quad (5)$$

As given in equation (4) and (5), K or Na vacancies (V'_K or V'_{Na}) are compensated by the creation of oxygen vacancies ($V^{\bullet\bullet}_O$) for charge neutralization. Hence, the intrinsic defects that may exist in KNL-NS ceramic are most likely cation vacancies (V'_K and V'_{Na}) and oxygen vacancies ($V^{\bullet\bullet}_O$). In perovskite-based materials, the cation vacancies have been reported as quenched defects at low temperature, becoming mobile at high temperature [28], Whereas, oxygen vacancies are the most mobile ionic species in perovskite lattice at room temperature

[29,30]. In PZT based-piezoelectrics, the pinning of domain walls by charged defect agglomerations, particularly oxygen vacancies, are considered as the primary cause for polarization loss during fatigue cycling [31-33]. A similar mechanism would sufficiently describe our observations in KLN-NS ceramic. During the ferroelectric polarization switching, charged defects such as oxygen vacancies are likely to move toward domain wall regions and cause an increased concentration of defects at this location, thereby agglomerations of defects are promoted [4,33-35]. This in turn results in the pinning of the ferroelectric domains, subsequently inhibiting domain switching and hence ferroelectric fatigue degradation.

When a small amount of 0.04Ta is added into the KNL-NST system, a higher reduction in $2P_r$ is observed. Although this sample exhibits a coexistence of two ferroelectric phases (orthorhombic and tetragonal), the lower fatigue resistance is observed. The observed result is similar to pervious work on the fatigue resistance of KNL-NS ceramics [9]. For bipolar fatigue studies, long term cycling with a bipolar electric field can lead to microscopic defect accumulation and/or defect clusters at domain walls [31,36-38] effectively pinning non-180° domain walls [39,40]. This behavior will be discussed later. Therefore, it is expected that there are more non-180° domain walls due to the coexistence of two ferroelectric phases, similar to what is observed in perovskite PZT systems with rhombohedral−tetragonal coexisting phases at room temperature [41]. The higher density of non-180° domain walls results in a strong pinning effect and a higher reduction of $2P_r$.

When the additional Ta concentration is increased to $x = 0.07$, a lower reduction of $2P_r$ is found. This implies that there is an increase in fatigue resistance for this composition. A lower density of non-180° domains would be expected as the main reason for an improvement of fatigue endurance. The tetragonal structure of this Ta doped sample has only 90° and 180°

domain walls with no additional non-180° domain walls to be pinned during continuous electric field switching, preventing loss of polarization. However, further addition of Ta (x = 0.11) into the KNL-NS system leads to a slight increase in the $2P_r$ reduction as compared to the sample with x = 0.07. Fatigue in this sample may be due to an increase of domain wall pining caused by an increase of *c/a*. It has been reported that the concentration of 90° domains (non-180° domains) depends on the tetragonality [42]. Namely, high *c/a* ratio induces the formation of more 90° domains. As shown in Fig. 1(b) and Table 1, it can be seen that both samples with 0.07 and 0.11 exhibit a tetragonal structure, but the values of the *c/a* ratio are different. The material with x = 0.11 is expected to have a higher 90° domain densities than the material with the lower value of *c/a*. 90^o domain walls are believed to be the perfect trapping sites for oxygen vacancies due to their high electrostrictive potential as reported by Y. Xiao and K. Bhattacharya [43]. They demonstrated that the potential drop across the 90^o domain wall is one order higher than the 180^o domain walls, implying that the 90^o domain walls have much larger electrical mismatch than 180^o domain walls. This electrical mismatch at the 90^o domain walls becomes the original site for oxygen vacancy trapping. When oxygen vacancies have highly accumulated at those sites, domain wall pinning are promoted and thus leads to the fatigue reduction. Therefore, domain wall pinning caused by the oxygen vacancy agglomerations is more pronounced in the sample with x = 0.11 and thereby a larger deterioration of polarization is observed in this sample than for the x = 0.07 composition. Furthermore, from Fig. 3, it can be observed that the remanent polarization ($2P_r$) of all KNL-NST$_x$ samples decreases roughly as an exponential decay function with the number of domain switches. This trend can be expressed using equation 6:

$$2P_r(N) = \mathrm{A}e^{(-\frac{N}{t})} + \mathrm{C} \tag{6}$$

Equation (6) suggests that the polarization ($2P_r$) directly depends on cycle number (N). If the cycle number is low, the domains are easily switched. Inversely, the domains are hindered to switch when the cycle number is high. The decay rate of ferroelectric polarization can be indicated by A and t which are the constant value of the exponential equation. The different compositions should have different decay rates. Additionally, C is a parameter that represents the maximum value of remanent polarization. These characteristics are the direct result of domain wall movement (or domain switching) behavior under cyclic electrical loading.

In order to investigate the influence of bipolar fatigue on phase evolution, X-ray diffraction of samples before electrical poling is compared with samples after electrical poling and after bipolar fatigue as illustrated in Fig. 4. The intensity ratios of the two important diffraction peaks at 44-48° are also listed in Table 3. In Fig. 4, it is found that the XRD patterns before and after electrical poling and after the fatigue process for all compositions have different intensity ratios as shown in Table 3. For the undoped sample, which exhibits an orthorhombic phase (x = 0), it should be noted that peak intensity ratio of $I_{(202)}/I_{(020)}$ increases after electrical poling; this is directly influenced by changes in the non-180° domain (e.g. 60°, 90° and 120° domains) orientation and/or crystallographic texture [44,45]. After the application of a cyclic field, the diffraction intensity ratio is nearly constant to that in the poled sample. However, the diffraction intensities of (202) and (020) peaks are less than that seen in in the poled state. This may indicate that the volume fraction of preferred domain orientation decreases since the domains cannot be reoriented parallel to the applied field direction due to domain pinning effect by charged defects such as oxygen vacancies. In the composition with x = 0.04 exhibiting a coexistence of two phases, the intensity ratio changes from approximately 1.0 (unpoled state) to 1.2 (after poling), which indicates that the poling increases the degree of the domain texture along the direction of

the field [46,47]. After applying the cyclic field to the poled sample, the intensity ratio is nearly the same as the poled state; however, the relative intensity of the lower 2θ and higher 2θ peaks decrease. This suggests that the electrical fatigue may induce a partial loss of domain texture in coexisting phases. In the case of the samples with tetragonal structure ($0.07 \leq x \leq 0.11$), the intensity ratio of $I_{(002)}/I_{(200)}$ increases after poling. It is assumed that the extensive 90° domain switching occurs in tetragonal samples during the poling process, which agrees with the previous reports [48,49]. After electrical fatigue, however, a reduction of $I_{(002)}/I_{(200)}$ intensity ratio is observed in both samples after fatigue. As compared to the poled state, there is a difference in rate reduction of $I_{(002)}/I_{(200)}$ peak intensity ratio between the compositions with $x = 0.07$ and 0.11. Namely, $I_{(002)}/I_{(200)}$ intensity ratio decreases slightly for the $x = 0.07$ composition, while there is a large reduction of $I_{(002)}/I_{(200)}$ peak intensity ratio in $x = 0.11$ sample. This phenomenon suggests that the 90° domains in $x = 0.11$ sample are more inhibited by defect accumulations and do not align as much with the direction of the cyclic field as for $x = 0.07$. This is consistent with the lower polarization degradation found in the $x = 0.07$. These observations show that the domain texture changes can be detected by X-ray diffraction technique. In addition, X-ray diffraction results are also in good agreement with the fatigue results.

Bipolar fatigue can also induce microstructural damage (i.e. cracks, melted layers, fractures) [4,50-52] in piezoelectric materials, especially in the region near the electrode. Thus, an experiment is carried out with a cross-section of the KNL-NST$_x$ top surface as shown in Fig. 5. Microstructure surfaces under the electrode before and after fatigue of KNL-NST$_x$ ceramics are then investigated as compared to unmodified KNL-NS as provided in Fig. 5. Representative SEM surfaces of unmodified KNL-NS show a damaged layer after the fatigue test. The formation of cracks in this sample is because of the strain incompatibility between the

ferroelectric bulk and the regions near the electrode during the fatigue test [53-57]. These strain mismatches can occur due to heterogeneous switching of domains [55]. The domain reorientation can generate a ferroelastic strain mismatch [58,59], leading to stress in the sample. The amount of stress in the sample is proportional to the magnitude of strain mismatch [60] and is a driving force for crack propagation [61]. In the unmodified composition, the domain walls are pinned by oxygen vacancies agglomeration. This leads to an inhibition of domain switching during the repeated field cycling, inducing a large residual ferroelastic strain incompatibility between pinned domains and neighboring switchable domains and hence resulting in a high internal stress concentration at domain walls [36,62]. When the internal stress concentration exceeds the elastic limit of the material, cracks are formed. Similar results are found in fatigued PZT-based [51,63] and some lead-free piezoelectric materials [50,64]. In these materials, cracking is frequently observed in the surface region underneath the electrode as a result of the heterogeneity of the mechanical stresses as compared to the bulk [52]. These cracks can lead to polarization loss [13,52,65-67]. The field screening effect [52] is a well-known theory, which can be used to explain the influence of the damaged microstructure on the switchable polarization of ferroelectric materials. Therefore, a similar mechanism would sufficiently describe our observations for the KNL-NS ceramic. As the cracking is present, an applied voltage would drop at the cracks, leading to a significant reduction in the effective electric field. The decrease in the effective field causes a decrease in the ability of some domains to switch and consequently a loss in polarization as depicted in Fig. 3.

By substituting 004Ta into KNL-NS ceramic, there is no cracking present on the surfaces after fatigue measurements. This observation indicates that bipolar fatigue of these ceramics is not influenced by the mechanism of microstructure damage. This result confirms that a large

amount of non-180° domains are pinned by oxygen vacancy accumulation which contributes to the change in polarization fatigue, as mentioned previously. Even though it is expected that this sample should have a large concentration of stresses due to the pinning effect, these stresses may not exceed the elastic limit of the sample. Instead, the pinning effect only results in loss of polarization. As reported in PZT ceramics, the effect of internal stresses is more pronounced in the regions further away from the MPB region [68]. In this case, therefore, a lower concentration of internal stresses caused by two-phase coexistence is assumed as a main cause for the disappearing of microstructural cracks. For more Ta-doped KNL-NS ($0.07 \leq x \leq 0.11$), the cross-sectional surfaces of unfatigued and fatigued samples show no differences. The lower pinning effect seems to be the most important mechanism for this result. The low number of locked domain walls leads to less residual stress mismatch and reduces the probability of crack propagation, giving less field screening. Thus, an increase in fatigue resistance is found for these compositions. As indicated by SEM, it is confirmed that bipolar fatigue leads to crack formation in the sample with $x = 0$ and consequently a corresponding loss in polarization whereas the cracking layer is not generated near the electrode/ferroelectric interfaces of the samples with xTa addition.

To describe the fatigue behavior of KNL-NST ceramics, a possible mechanism based on the relationship of domain wall motion and defects is created as provided in Fig. 6. In the situation without an applied electric field, the domains are randomly orientated as shown in Fig. 6(a), thereby the net polarization is zero. During the sintering process, intrinsic defects are generated. In our KNL-NST$_x$ samples, alkaline (K and Na vacancies) and oxygen vacancies are expected to form due to the loss of Na and K. An analysis of charge transportation in typical perovskite materials indicates that the oxygen vacancies are the only point defects, which have significant

mobility [69]. Therefore, the main defects under consideration in this model are oxygen vacancies. These oxygen vacancies are easily moved by the field generated by the spontaneous polarization. They are then trapped at domain boundaries and subsequently pinned to the domain walls as shown in Fig 6(a). However, there is a little interaction between oxygen vacancies and 180^{o} domain walls. This is due to the positive and negative polarization charges distributed equally on each side of a 180^{o} domain wall, thereby not producing a potential difference. Thus, oxygen vacancies do not move to this region and 180^{o} domain walls are not pinned [70]. However, the 180° domain walls can be pinned by defects if the domain wall becomes distorted [39,40]. In contrast for non-180^{o} domain walls, there is an imbalance of positive and negative charges across the domain boundary. This induces a potential difference regardless of the presence of oxygen vacancies at this region. When the material is subjected to a sufficiently high DC field (called poling process), the domains are aligned in the direction of the electric field as depicted in Fig. 6(b). As stated earlier, 180° domain walls are weakly pinned by oxygen vacancies, so that they are easily depinned by an applied external electric field. When the DC field is off, most dipoles are roughly oriented in the same direction. A long-term AC electric field is then applied to the poled sample. Since oxygen vacancies are highly mobile under an applied electric field, the distribution of oxygen vacancies changes during the electrical fatigue cycling [38]. Due to the repeated domain switching, oxygen vacancies are likely to move towards non 180°domain walls. This leads to an accumulation of defects at those sites with increasing cycling numbers, resulting in the strong pinning of domain walls [31,33] as shown in Fig. 6(c). Oxygen vacancy accumulation prevents the domains from switching [33], hence a polarization reduction is observed. In contrast, due to the weak pinning of 180° domain walls, these domains can be switched easily by an applied cycling electric field.

Based on this model, the influential factors on the electrical fatigue in KNL-NST$_x$ system resulting from long-term bipolar cycling may be divided into two components, namely the concentration of non-180° domain walls and oxygen vacancy accumulation. The sample with a high density of non-180° domain walls shows a greater loss of polarization due to stronger domain wall pinning. A high number of pinned domains contributes to the limitation of domain switching. The limited switching obviously gives rise to stresses between non-switched domains and their neighboring domains [36]. If the stress density is higher than the elastic limit of the sample, microstructural damage (i.e. cracking) occurs. However, if the concentration of stresses does not exceed the elastic limit, the cracks are not present. In contrast, the sample with a low amount of non-180° domain walls show less domain wall pinning, which results in less stress formation.

4. Conclusions

The fatigue behavior of unmodified KNL-NS is compared to that of *x*Ta doped KNL-NS. Phase characterization of the ceramics reveals a phase transformation from orthorhombic to tetragonal for Ta ≥ 0.04. Bipolar fatigue measurements suggest that an unmodified sample shows low fatigue resistance, which is due to the formation of oxygen vacancies. Under fatigue cycling, the ferroelectric domains could be pinned by these oxygen vacancies, inhibiting domain switching and loss of polarization is observed. Addition of Ta enhances the fatigue endurance. This fatigue improvement is mainly due to a reduction in the pinning to ferroelectric domain walls as a result of low content of non-180° domain walls in compositions with a tetragonal structure. This suggests that the Ta doped samples are more stable under a continuous cyclic load compared to the unmodified sample. It can be concluded that the phase change from

orthorhombic in undoped KNL-NS to tetragonal in Ta doped samples has a significant effect on the enhancement of bipolar electric fatigue resistance. The results in this research provide valuable knowledge for the design and development of new lead free KNN-based ferroelectric ceramics in the future.

Acknowledgements

This work is supported by Suranaree University of Technology (SUT) and by Office of the Higher Education Commission under NRU Project of Thailand.

References

[1] G.H. Haertling, Ferroelectric ceramics: history and technology, J. Am. Ceram. Soc. 82 (1999) 797–818.

[2] J.F. Scott, Ferroelectric Memories, Springer, Heidelberg, 2000.

[3] K. Uchino, Piezoelectric Actuators and Ultrasonic Motors, Kluwer Academic Publishers, London, 1997.

[4] J. Nuffer, D.C. Lupascu, J. Rödel, Damage evolution in ferroelectric PZT induced by bipolar electric cycling, Acta Mater. 48 (2000) 3783–3794.

[5] J. Rödel, W. Jo, K.T.P. Seifert, E.-M. Anton, T. Granzow, D. Damjanovic, Perspective on the development of lead-free piezoceramics, J. Am. Ceram. Soc. 92 (2009) 1153–1177.

[6] L. Egerton, D.M. Dillon, Piezoelectric and dielectric properties of ceramics in the system potassium–sodium niobate, J. Am. Ceram. Soc. 42 (1959) 438–442.

[7] G.-Z. Zang, J.-F. Wang, H.-C. Chen, W.-B. Su, C.-M. Wang, P. Qi, B.-Q. Ming, J. Du, L.-M. Zheng, S. Zhang, T.R. Shrout, Perovskite $(Na_{0.5}K_{0.5})_{1-x}(LiSb)_xNb_{1-x}O_3$ lead-free piezoceramics, Appl. Phys. Lett. 88 (2006) 212908–1–3.

[8] Y. Saito, H. Takao, T. Tani, T. Nonoyama, K. Takatori, T. Homma, T. Nagaya, M. Nakamura, Lead-free piezoceramics, Nature. 432 (2004) 84–87.

[9] S. Zhang, R. Xia, H. Hao, H. Liu, T.R. Shrout, Mitigation of thermal and fatigue behavior in $K_{0.5}Na_{0.5}NbO_3$-based lead free piezoceramics, Appl. Phys. Lett. 92 (2008) 152904–1–3.

[10] Z. Yang, Y. Chang, L. Wei, Phase transitional behavior and electrical properties of lead-Free $(K_{0.44}Na_{0.52}Li_{0.04})(Nb_{0.96-x}Ta_xSb_{0.04})O_3$ piezoelectric ceramics, Appl. Phys. Lett. 90 (2007) 042911–1–3.

[11] C. Uthaisar, P. Kantha, R. Yimnirun, S. Pojprapai, Integr. Ferroelectr. Lead-free $(K_{0.50}Na_{0.46}Li_{0.04})(Nb_{(0.96-x)}Sb_{0.04}Ta_x)O_3$ ceramics on piezoelectric properties, 149 (2013) 114–120.

[12] C.B. Sawyer, C.H. Tower, Rochelle Salt as a Dielectric, Phys. Rev. 35 (1930) 269–273.

[13] Q.Y. Jiang, E.C. Subbarao, L.E. Cross, Effect of composition and temperature on electric fatigue of La-doped lead zirconate titanate ceramics, J. Appl. Phys. 75 (1994) 7433–7442.

[14] Y. Guo, K. Kakimoto, H. Ohsato, Phase transitional behavior and piezoelectric properties of $(Na_{0.5}K_{0.5})NbO_3$–$LiNbO_3$ ceramics, Appl. Phys. Lett. 85 (2004) 4121–4123.

[15] The Joint Committee on Powder Diffraction Standards (JCPDS) file number 71-0945.

[16] The Joint Committee on Powder Diffraction Standards (JCPDS) file number 71-2171.

[17] M.-P. Chun, K.-M. Kang, J.-H. Cho, B.-I. Kim, Effect of the firing conditions on the phase formation of alkali metal niobate piezoelectric ceramics, J. Korean. Phys. Soc. 59 (2011) 2583–2588.

[18] J. Zeng, Y. Zhang, L. Zheng, G. Li, Q. Yin, Enhanced ferroelectric properties of potassium sodium niobate ceramics modified by small amount of $K_3Li_2Nb_5O_{15}$, J. Am. Ceram. Soc. 92 (2009) 752–754.

[19] Y. Wang, Y. Lu, M. Wu, D. Wang, Y. Li, Phase structure and enhanced piezoelectric properties of lead-free ceramics (1-x)($K_{0.48}Na_{0.52}$)NbO_3–(x/5.15) $K_{2.9}Li_{1.95}Nb_{5.15}O_{15.3}$ with high curie temperature, Int. J. Appl. Ceram. Technol. 9 (2012) 221–227.

[20] K. Wang, J. Li, Domain engineering of lead-free Li-modified (K,Na)NbO_3 polycrystals with highly enhanced piezoelectricity, Adv. Funct. Mater. 20 (2010) 1924–1929.

[22] J.-J. Zhou, K. Wang, F. Li, J.-F. Li, X.-W. Zhang, Q.-M. Wang, High and frequency insensitive converse piezoelectric coefficient obtained in $AgSbO_3$-modified (Li, K, Na)(Nb, Ta)O_3 lead-free piezoceramics, J. Am. Ceram. Soc. 96 (2013) 519–523.

[23] J. Wang, L. Luo, Y. Huang, W. Li, Effect of Yb codoping on the phase transition, and electrical and photoluminescence properties in KNLN:Er/xYb ceramics, J. Am. Ceram. Soc. 99 (2016) 1625–1630.

[24] H. Wang, D. Ruan, Y.-J. Dai, X.-W. Zhang, Relationship between phase structure and electrical properties of ($K_{0.5}Na_{0.5}$)NbO_3–$LiTaO_3$ lead-free ceramics, Curr. Appl. Phys. 12 (2012) 504–508.

[25] R.D. Shanon, Revised effective ionic radii and systematic studies of interatomie distances in halides and chaleogenides, Acta Cryst. A32 (1976) 751−767.

[26] X.J. Lou, Polarization fatigue in ferroelectric thin films and related materials, J. Appl. Phys. 105 (2009) 024101–1–24.

[27] M.A. Rafiq, A. Tkach, M.E. Costa, P.M. Vilarinho, Defects and charge transport in Mn-doped $K_{0.5}Na_{0.5}NbO_3$ ceramics, Phys. Chem. Chem. Phys. 17 (2015) 24403–24411.

[28] B. Guiffard, E. Boucher, L. Eyraud, L. Lebrun, D. Guyomar, Influence of donor co-doping by niobium or fluorine on the conductivity of Mn doped and Mg doped PZT ceramics, J. Euro. Ceram. Soc. 25 (2005) 2487–2490.

[29] T. Kudo, H. Obayashi, T. Gejo, Electrochemical behavior of the perovskite-type $Nd_{1-x}Sr_xCoO_3$ in an aqueous alkaline solution, J. Electrochem. Soc. 122 (1975) 159–163.

[30] T. Kudo, H. Obayashi, M. Yoshida, Rare earth cobaltites as oxygen electrode materials for alkaline solution, J. Electrochem. Soc. 124 (1977) 321–325.

[31] J.F. Scott, M. Dawber, Oxygen-vacancy ordering as a fatigue mechanism in perovskite ferroelectrics, Appl. Phys. Lett. 76 (2000) 3801–3803.

[32] I.K. Yoo, S.B. Desu, Fatigue modeling of lead zirconate titanate thin films, Mater. Sci. Eng. BI3 (1993) 319–322.

[33] C. Brennan, Model of ferroelectric fatigue due to defect/domain interactions, Ferroelectrics. 150 (1993) 199–208.

[34] J.F. Scott, C.A. Araujo, B.M. Melnick, L.D. McMillan, R. Zuleeg, Quantitative measurement of space-charge effects in lead zirconate-titanate memories, J. Appl. Phys. 70 (1991) 382–388.

[35] M.-J. Pan, S.-E. Park, C.W. Park, K.A. Markowski, S. Yoshikawa, C.A. Randall, Superoxidation and electrochemical reactions during switching in $Pb(Zr,Ti)O_3$ Ceramics, J. Am. Ceram. Soc. 79 (1996) 2971–2974.

[36] V.V. Shvartsman, A.L. Kholkin, C. Verdier, Z. Yong, D.C. Lupascu, Investigation of fatigue mechanism in ferroelectric ceramic via piezoresponse force microscopy, J. Eur. Ceram. Soc. 25 (2005) 2559–2561.

[37] D.C. Lupascu, Fatigue in ferroelectric ceramics due to cluster growth, Solid State Ionics. 177 (2006) 3161–3170.

[38] D.C. Lupascu, Fatigue in Ferroelectric Ceramics and Related Issues, Springer, New York, 2004.

[39] Y. Xiao, V.B. Shenoy, K. Bhattacharya, Depletion layers and domain walls in semiconducting ferroelectric thin films, Phys. Rev. Lett. 95 (2005) 247603–1–4.

[40] Y. Su, C.M. Landis, Continuum thermodynamics of ferroelectric domain evolution: theory, finite element implementation, and application to domain wall pinning, J. Mech. Phys. Solids 55 (2007) 280–305.

[41] J.Y. Li, R.C. Rogan, E. Ustundag, K. Bhattacharya, Domain switching in polycrystalline ferroelectric ceramics, Nat. Mater. 4 (2005) 776–781.

[42] J. Fu, R. Zuo, X. Wang, L. Li, Phase transition characteristics and piezoelectric properties of compositionally optimized alkaline niobate based ceramics, J. Alloy Compd. 486 (2009) 790–794.

[43] Y. Xiao and K. Bhattacharya, Interaction of oxygen vacancies with domain walls and its impact on fatigue in ferroelectric thin films, Proc. of SPIE. 5387 (2004) 354–365.

[44] J.L. Jones, E.B. Slamovich, K.J. Bowman, Domain texture distributions in tetragonal lead zirconate titanate by X-ray and neutron diffraction, J. Appl. Phys. 97 (2005) 034113–1–6.

[45] C. Bedoya, C. Muller, J.L. Baudour, V. Madigou, M. Anne, M. Roubin, Sr-doped $PbZr_{1-x}Ti_xO_3$ ceramic: structural study and field-induced reorientation of ferroelectric domains, Mater. Sci. Eng. 75 (2000) 43–52.

[46] M.C. Ehmke, S.N. Ehrlich, J.E. Blendell, K.J. Bowman, Phase coexistence and ferroelastic texture in high strain $(1-x)Ba(Zr_{0.2}Ti_{0.8})O_3–x(Ba_{0.7}Ca_{0.3})TiO_3$ piezoceramics, J. Appl. Phys. 111 (2012) 124110−1−7.

[47] H. Fan, H.E. Kim, Perovskite stabilization and electromechanical properties of polycrystalline lead zinc niobate–lead zirconate titanate, J. Appl. Phys. 91 (2002) 317−322.

[48] D.A. Hall, A. Steuwer, B. Cherdhirunkorn, T. Mori, P.J. Withers, A high energy synchrotron X-ray study of crystallographic texture and lattice strain in soft lead zirconate titanate ceramics, J. Appl. Phys. 96 (2004) 4245−4252.

[49] M. Liu, K.J. Hsia, M.R. Sardela, In situ X-Ray diffraction study of electric-field-induced domain switching and phase transition in PZT-5H, J. Am. Ceram. Soc. 88 (2005) 210–215.

[50] Z. Luo, J. Glaum, T. Granzow, W. Jo, R. Dittmer, M. Hoffman, J. Rödel, Bipolar and unipolar fatigue of ferroelectric BNT-based lead-free piezoceramics, J. Am. Ceram. Soc. 94 (2011) 529–535.

[51] Z. Luo, S. Pojprapai, J. Glaum, M. Hoffman, Electrical fatigue-induced cracking in lead zirconate titanate piezoelectric ceramic and its influence quantitatively analyzed by refatigue method, J. Am. Ceram. Soc. 95 (2012) 2593–2600.

[52] N. Balke, H. Kungl, T. Granzow, D.C. Lupascu, M.J. Hoffmann, J. Rödel, Bipolar fatigue caused by field screening in $Pb(Zr,Ti)O_3$ ceramics, J. Am. Ceram. Soc. 90 (2007) 3869–3874.

[53] J. Nuffer, D.C. Lupascu, J. Rödel, Microcrack clouds in fatigued electrostrictive 9.5/65/35 PLZT, J. Eur. Ceram. Soc. 21 (2001) 1421–1423.

[54] C. Verdier, F.D. Morrison, D.C. Lupascu, J.F. Scott, Fatigue studies in compensated Bulk Lead Zirconate Tiatante, J. Appl. Phys. 97 (2005) 024107–1–6.

[55] Q.Y. Jiang, E.C. Subbarao, L.E. Cross, Grain size dependence of electric fatigue behavior of hot pressed PLZT ferroelectric ceramics, Acta Metall. Mater. 42 (1994) 3687–3694.

[56] S. Winzer, N. Shankar, A.P. Ritter, Designing cofied multilayer electrostrictive actuators for reliability, J. Am. Ceram. Soc. 72 (1989) 2246–2257.

[57] J. Shieh, J.E. Huber, N.A. Fleck, Fatigue crack growth in ferroelectrics under electrical loading, J. Euro. Ceram. Soc. 26 (2006) 95–109.

[58] S. Pojprapai (Imlao), J.L. Jones, A.J. Studer, J. Russell, N. Valanoor, M. Hoffman, Ferroelastic domain switching fatigue in lead zirconate titanate ceramics, Acta Mater. 56 (2008) 1577–1587.

[59] S. Pojprapai, J. Russell, H. Manc, J.L. Jones, J.E. Daniels, M. Hoffman, Frequency effects on fatigue crack growth and crack tip domain-switching behavior in a lead zirconate titanate ceramic, Acta Mater. 57(13) (2009) 3932–3940.

[60] W. Yang, Electric induced failure mechanism, Adv. Mechanics. 26 (1996) 338–352.

[61] D.A. Hall, T. Mori, T.P. Comyn, E. Ringgaard, J.P. Wright, Residual stress relief due to fatigue in tetragonal lead zirconate titanate ceramics, J. Appl. Phys. 114 (2012) 024103–1–6.

[62] Y. Zhang, D.C. Lupascu, E. Aulbach, I. Baturin, Heterogeneity of fatigue in bulk lead zirconate titanate, A. Bell, J. Rödel, Acta Mater. 53 (2005) 2203–2213.

[63] O. Namsar, S. Pojprapai, A. Watcharapasorn, S. Jiansirisomboon, Enhancement of fatigue endurance in ferroelectric PZT ceramic by the addition of bismuth layered SBT, J. Appl. Phys. 116 (2014) 164105–1–7.

[64] S.-C. Lu, Y.-H. Chen, W.-H. Tuan, J. Shieh, C.-Y. Chen, Effect of microstructure on dielectric and fatigue strengths of $BaTiO_3$, J. Eur. Ceram. Soc. 30 (2010) 2569–2576.

[65] H. Cao, A.G. Evans, Electric-field-induced fatigue crack growth in piezoelectrics, J. Am. Ceram. Soc. 77 (1994) 1783–1786.

[66] J. Nuffer, D.C. Lupascu, A. Glazounov, H.-J. Kleebe, J. Rödel, Microstructural modifications of ferroelectric lead zirconate titanate ceramics due to bipolar electric fatigue, J. Eur. Ceram. Soc. 22 (2002) 2133–2142.

[67] E.C. Subbarao, V. Srikanth, W. Cao, L.E. Cross, Domain switching and microcracking during poling of lead zirconate titanate ceramics, Ferroelectrics. 145 (1993) 271–281.

[68] S.W. Freiman, L. Chuck, J.J. Mecholsky, D.L. Shelleman, L.J. Storz, Fracture mechanisms in lead zirconate titanate ceramics, Fract. Mech. Ceram. 8 (1986) 175–185.

[69] M.V. Ramond, D.M. Smyth, Defects and charge transport in perovskite ferroelectrics, J. Phys. Chem. Solids. 57 (1996) 1507−1511.

[70] L. Hong, A.K. Soh, Q.G. Du, J.Y. Li, Interaction of O vacancies and domain structures in single crystal $BaTiO_3$: Two-dimensional ferroelectric model, Phys. Rev. B 77 (2008) 094104−1−7.

Figure Captions

Fig. 1. (a) Room temperature XRD patterns of KNL-NST$_x$ ceramics at 44–48° and (b) the variation of the crystal structure parameters of KNL-NST$_x$ ceramics as a function of x.

Fig. 2. P-E loops of KNL-NST$_x$ ceramics at 1 cycle, 5 x 10^4 and 1 x 10^6 cycles.

Fig. 3. The average $2P_r(N)/2P_r(0)$ as a function of bipolar cycles of KNL-NST$_x$ ceramics with different xTa concentration. The dash lines are fitted by using equation (6).

Fig. 4. X-ray diffraction data of $(202)_O$:$(020)_O$ or $(002)_T$:$(200)_T$ reflections for KNL-NST$_x$ ceramics before and after electrical poling and after fatigue process.

Fig. 5. Cross-sectional surfaces underneath electrode/bulk ferroelectric interfaces before and after fatigue of KNL-NST$_x$ ceramics.

Fig. 6. Illustration of possible fatigue mechanism based on the domain switching (motion of domain walls) and oxygen vacancy accumulation.

Fig. 1.

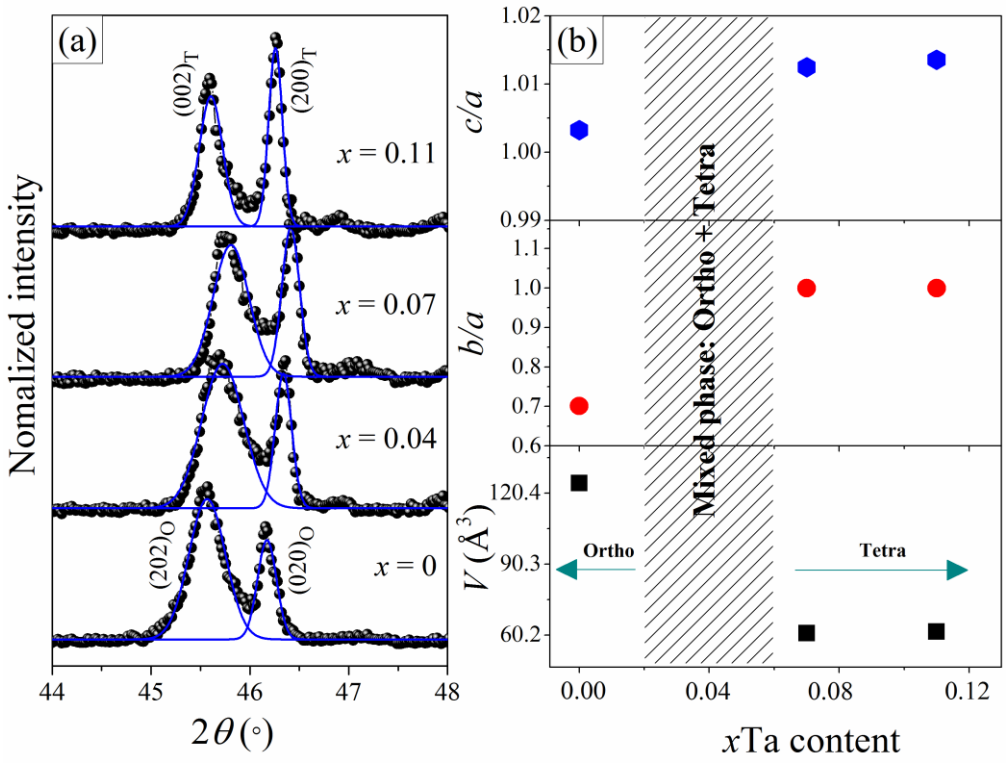
(a)
(002)T
(200)T
x = 0.11
x = 0.07
x = 0.04
x = 0
(202)O
(020)O
Nomalized intensity
2θ (°)
(b)
c/a
b/a
V (Å3)
Mixed phase: Ortho + Tetra
Ortho
Tetra
xTa content

Fig. 2.

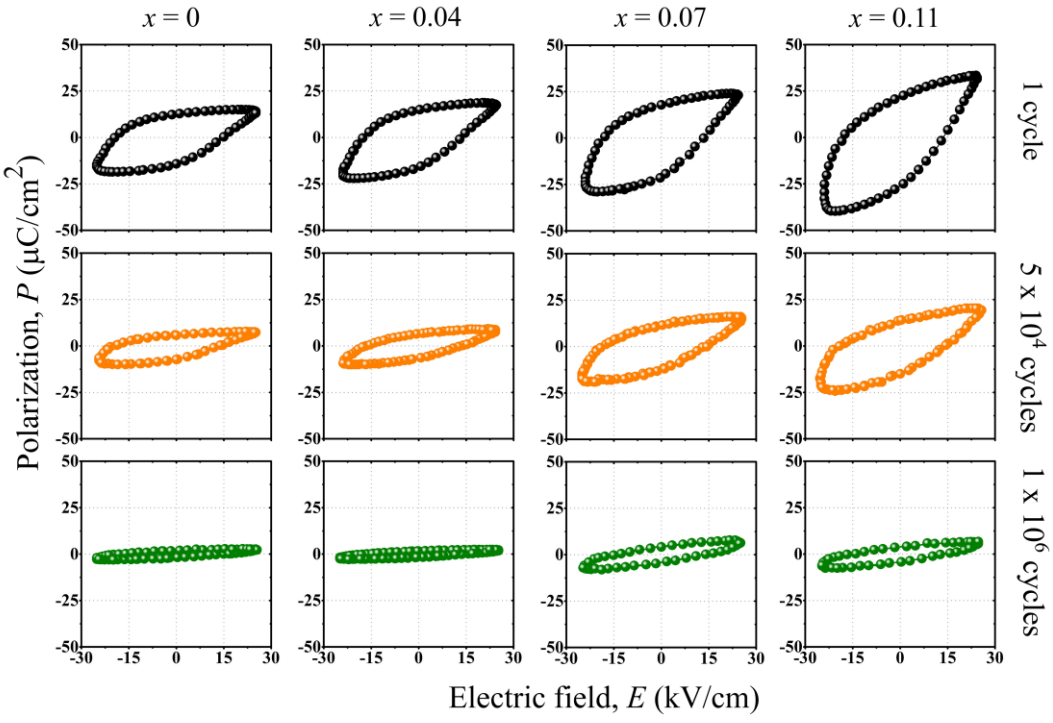
x = 0
x = 0.04
x = 0.07
x = 0.11
1 cycle
5 x 10^4 cycles
1 x 10^6 cycles
Polarization, P (μC/cm2)
Electric field, E (kV/cm)

Fig. 3.

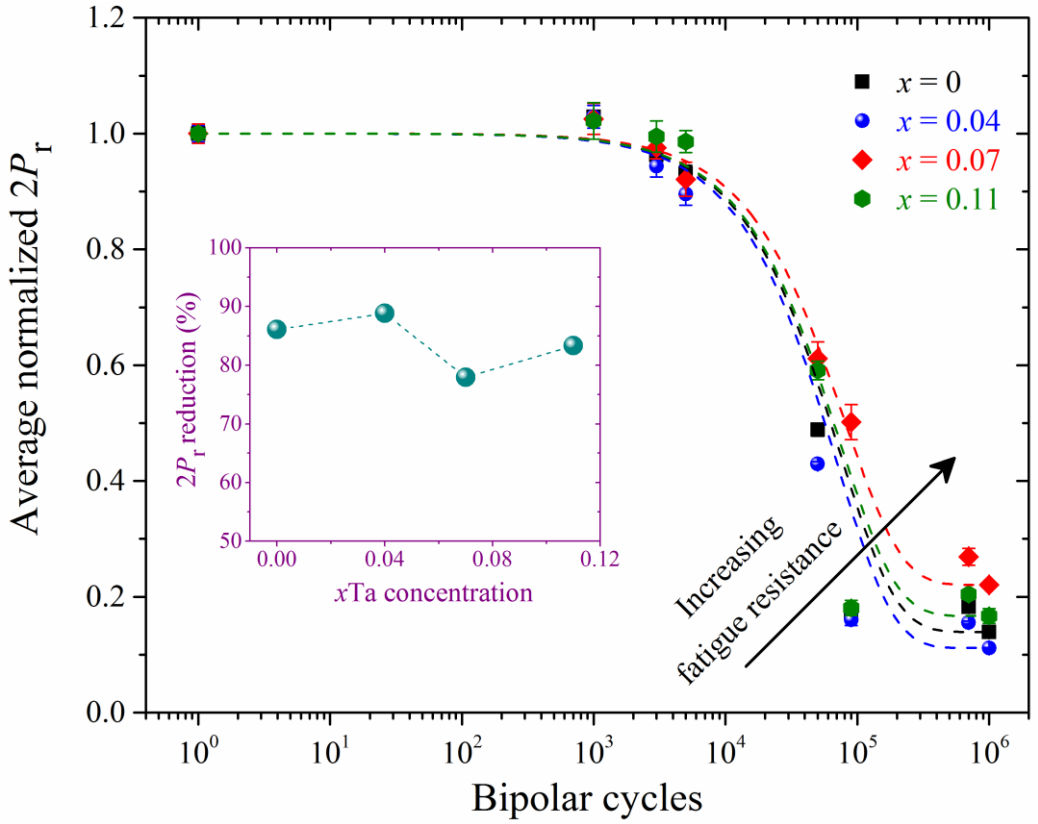
Average normalized $2P_r$
Bipolar cycles
$x = 0$
$x = 0.04$
$x = 0.07$
$x = 0.11$
$2P_r$ reduction (%)
xTa concentration
Increasing fatigue resistance

Fig. 4.

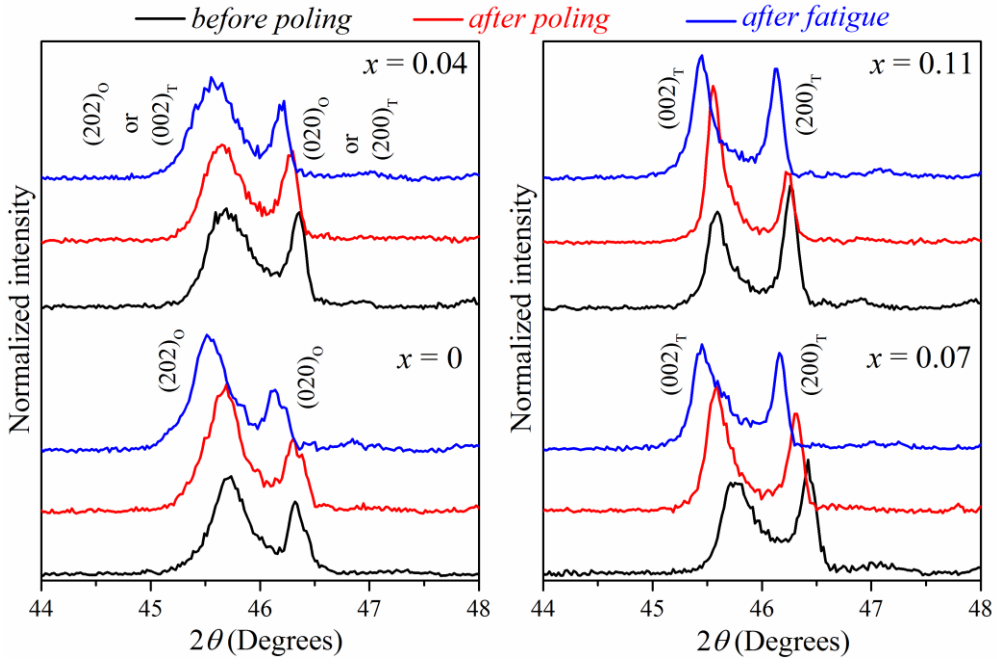
before poling
after poling
after fatigue
$x = 0.04$
$x = 0$
$x = 0.11$
$x = 0.07$
Normalized intensity
2θ (Degrees)

Fig. 5.

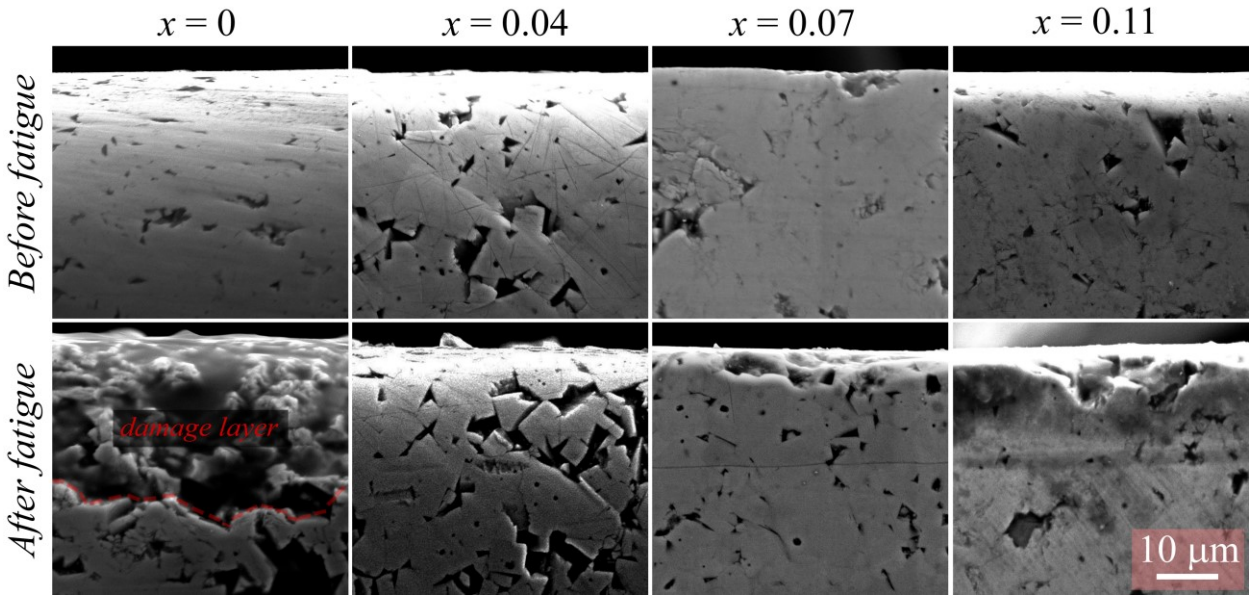
x = 0
x = 0.04
x = 0.07
x = 0.11
Before fatigue
After fatigue
damage layer
10 μm

Fig. 6.

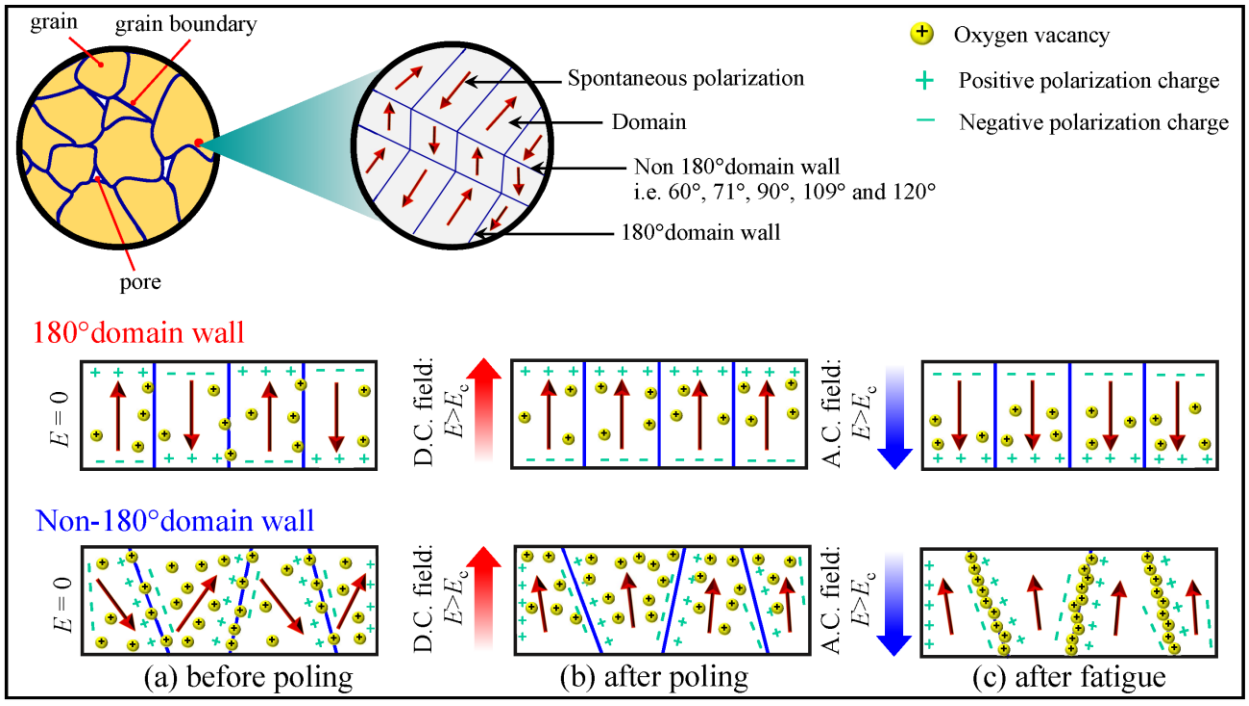
grain
grain boundary
pore
Spontaneous polarization
Domain
Non 180°domain wall
i.e. 60°, 71°, 90°, 109° and 120°
180°domain wall
Oxygen vacancy
Positive polarization charge
Negative polarization charge
180°domain wall
Non-180°domain wall
E = 0
D.C. field: E>Ec
A.C. field: E>Ec
(a) before poling
(b) after poling
(c) after fatigue

Table Captions

Table 1 Crystal parameters of KNL-NST$_x$ ceramics.

Table 2 The fitting parameters obtained from $2P_r(N)/2P_r(0)$ vs bipolar cycles (Fig. 3).

Table 3 Peak intensity ratio of $(202)_O$:$(020)_O$ or $(002)_T$:$(200)_T$ reflections of KNL-NST$_x$ ceramics before poling, after poling and after fatigue measurement.

Table 1

*x*Ta	Crystal structure	Lattice parameters (Å)			*V* (Å^3)	*c/a*	*b/a*	Peak intensity ratio Lower 2θ : Higher 2θ
		a	*b*	*c*				
0	Ortho	5.6153	3.9386	5.6336	124.5949	1.0032	0.7014	2.2:1.6 ≈ 1.4
0.04	Ortho + Tetra	-	-	-	-	-	-	2.2:2.1 ≈ 1.0
0.07	Tetra	3.9193	3.9193	3.9682	60.9550	1.0125	1.0000	2.1:2.6 ≈ 0.8
0.11	Tetra	3.9316	3.9316	3.9850	61.5988	1.0137	1.0000	2.1:2.7 ≈ 0.8

V = unit cell volume, *c/a* is tetragonality and *b/a* is orthorhombicity.

Table 2

*x*Ta content	*A*	*t*	*C*
0	0.8931	1.98 x 10^4	0.1676
0.04	0.8842	4.68 x 10^4	0.1140
0.07	0.7294	5.72 x 10^4	0.2245
0.11	0.8130	2.26 x 10^4	0.1923

Table 3

*x*Ta content	$I_{(202)}/I_{(020)}$ or $I_{(002)}/I_{(200)}$		
	Before poling	After poling	After fatigue
0	2.2:1.6 ≈ 1.4	2.8:1.6 ≈ 1.8	2.6:1.4 ≈ 1.8
0.04	2.2:2.1 ≈ 1.0	2.2:1.9 ≈ 1.2	2.1:1.7 ≈ 1.2
0.07	2.1:2.6 ≈ 0.8	2.9:2.3 ≈ 1.3	2.3:2.2 ≈ 1.1
0.11	2.1:2.7 ≈ 0.8	3.5:1.6 ≈ 2.2	2.7:2.4 ≈ 1.0